A Diagnostic Study of the Extratropical Precipitation Resulting from Tropical Cyclone Bola

MARK R. SINCLAIR

National Institute of Water and Atmospheric Research, Wellington, New Zealand

(Manuscript received 5 October 1992, in final form 20 March 1993)

ABSTRACT

This is the second of two papers on tropical storms entering middle latitudes in the southwest Pacific. This study focuses on the heavy rainfall associated with Tropical Cyclone Bola during 6–8 March 1988 following its passage from the tropics to a position near northern New Zealand. The heaviest precipitation fell on the upwind side of the Gisborne Ranges, where 5-day rainfall totals exceeding 800 mm were recorded.

Precipitation diagnoses from the 2.5° × 2.5° ECMWF dataset seriously underestimated the intensity of observed rainfall over the mountainous terrain. This failure resulted primarily from an inability to resolve the large orographic component of this rainfall. A simple scheme, based on ascent caused by flow over topography, was able to replicate the huge rainfall amounts on the upwind side of the mountain only when details of the local topography to approximately 10 km were included.

A quasigeostrophic ω diagnosis from the ECMWF data showed that large-scale ascent occurred where upper-level vorticity advection and increasing low-level thermal advection acted in phase. Strongest ascent occurred in the region between the difluent exit region of a westerly jet to the north of Bola and the confluent entrance to a second jet southeast of the South Island of New Zealand. A cross section revealed an associated two-cell vertical circulation pattern similar to that observed in other parts of the world. The heavy rain occurred just downstream from a low-level confluence where tropical air from Bola's eastern flank met cooler air from the southeast. Frontogenesis and moisture convergence associated with this confluence possibly helped to focus ascent near the Gisborne Ranges, although this could not be confirmed, because of the lack of observations.

1. Introduction

Tropical Cyclone Bola (March 1988) was one of the most destructive storms ever to strike New Zealand, bringing the heaviest rain in living memory to the north of the country. This study uses a combination of observations and European Centre for Medium-Range Weather Forecasts (ECMWF) initialized analyses to describe this event and to estimate the important dynamic and thermodynamic processes associated with the heavy rain. This paper is the second of two on tropical storms entering middle latitudes in the southwest Pacific. The first case study (Sinclair 1992) examined the structure and motion changes prior to and during the extratropical transition (ET) of Tropical Cyclone Patsy in December 1986. In contrast, the present study focuses on the behavior of Tropical Cyclone Bola *following* ET.

Tropical cyclone (TC) remnants are often associated with extreme precipitation in middle latitudes in the summer and autumn months. Tropical Storm Agnes (June 1972) produced one of the worst natural flood disasters in United States history (DeAngelis and Hodge 1972). Bosart and Carr (1978) attributed the severity of this event to the persistence of strong moisture convergence in high-θ_w air over mountainous terrain east of a slow-moving TC remnant, while Bosart and Dean (1991) demonstrated the importance of a subsynoptic-scale surface baroclinic zone in determining the location of the heavy rain. Aloft, DiMego and Bosart (1982a) noted a double jet configuration known to accompany vigorous tropospheric ascent (e.g., Uccellini and Kocin 1987).

The purpose of the present paper is (i) to document the heavy rainfall and describe the synoptic environment in which it fell, and (ii) to understand the observable physical processes responsible for the rain. Initialized analyses from ECMWF on a 2.5° latitude–longitude grid, augmented by available observations, are used to determine the structure of Bola during the period of heavy rain and to determine the important physical processes that favor vigorous ascent. Results are compared with previous studies of Northern Hemisphere (NH) transformation events.

Objectively analyzed datasets were used successfully by Carr and Bosart (1978) and DiMego and Bosart (1982b) to examine Agnes' rainfall. They were aided by plentiful data for both diagnosis and verification over the continental United States. Since the realism of operationally analyzed fields can be questionable

Corresponding author address: Dr. Mark R. Sinclair, National Institute of Water and Atmospheric Research, P.O. Box 3047, Wellington, New Zealand.

over data-sparse regions of the Southern Hemisphere (SH), the ability of the ECMWF fields to realistically diagnose the observed Bola rainfall will be evaluated. Unfortunately, we will show that such comparisons are made difficult here by an absence of rainfall observations over much of the storm area and are further complicated by very large rainfall variations caused by New Zealand's rugged terrain.

The next section provides the synoptic setting for this event, along with details of the observed rainfall. In section 3, the predictability of Bola's rainfall will be explored by estimating precipitation rates using standard methods on ECMWF fields and by comparing it with actual storm rainfall. This includes a simple method to estimate orographic precipitation over mountainous terrain. The operation of dynamic and thermodynamic processes that favor ascent will be described in section 4. A summary of results and concluding remarks are contained in section 5.

2. Storm overview

Of the nine or so tropical cyclones that form in the Southwest Pacific region each year (Revell 1981), about one to two of these can be expected to migrate to within 100 km of New Zealand. These usually bring substantial rain and, occasionally, high winds. Many of New Zealand's most memorable weather events are associated with such storms of tropical origin. In April 1968, a tropical disturbance reintensified dramatically as it approached New Zealand, causing winds gusting to 75 m s^{-1} near Wellington and resulting in the sinking of the interisland ferry *Wahine,* with the loss of 51 lives (Hill 1970). In March 1975, Tropical Cyclone Alison brought high winds and heavy rain to central parts of New Zealand, with 155 mm of rain recorded in 6 h at one South Island (SI) coastal location (Tomlinson 1975). Tropical Cyclone Bernie caused unprecedented wind damage to exotic forest production on the North Island (NI) in April 1982 (Littlejohn 1984).

The subject of the present study, Tropical Cyclone Bola, produced some of the largest precipitation totals for any single storm ever recorded on the NI. Bola's path toward New Zealand is shown in Fig. 1. After forming north of Fiji on 24 February 1988 and intensifying to hurricane strength over the next few days, Bola looped in the vicinity of Vanuatu where it caused widespread damage before accelerating poleward toward New Zealand during 2–5 March. During this period, Bola lost its characteristic TC appearance, as viewed from satellite imagery (not shown), and rapidly acquired asymmetries typical of extratropical cyclones.

From about 6 March, Bola became slow moving over the seas to the north of the NI. During this time, easterly gales and heavy rain lashed wide areas of northern New Zealand. Most of the storm damage arose from excessive rainfall in the Gisborne region (see Fig. 1), where precipitation totals over this 4-day

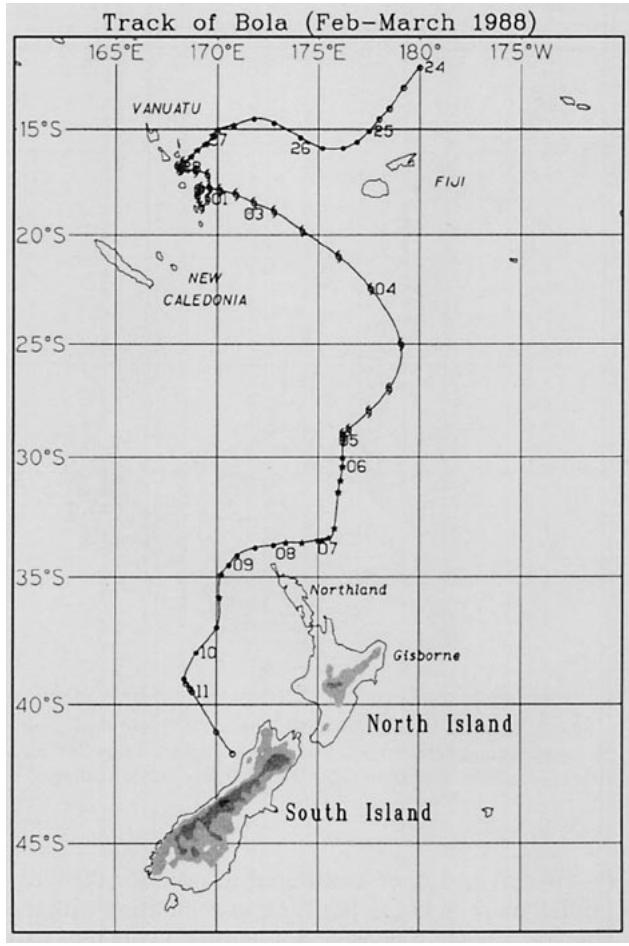

FIG. 1. Best track (solid line) for Bola, drawn from data in New Zealand Meteorological Service TC archive. Open circles represent maximum sustained wind speeds up to 17 m s^{-1}; filled circles—speeds between 18 and 23 m s^{-1}; stars—speeds between 24 and 33 m s^{-1}; and hurricane symbols—speeds greater than 33 m s^{-1}. These symbols are plotted every 6 h, with dates (February–March 1988) at 0000 UTC annotated nearest the symbol for that time. Places referred to in the text are also included.

period exceeded 600 mm over the inland high country, with several stations recording more than 800 mm. Many roads and bridges were washed out, and extensive damage was caused to buildings, roads, and pasture. Winds gusting to hurricane force damaged homes and production forests in other NI areas. This study will primarily address this period of severe weather over the NI.

a. Observed rainfall

Data from a network of raingages (Fig. 2) were used to determine the distribution of rainfall over the NI (Fig. 3). Twenty-four-hour rainfall totals, read at 0900 LST (2000 UTC) on the following day for the stations shown in Fig. 2, were Cressman analyzed onto a regular

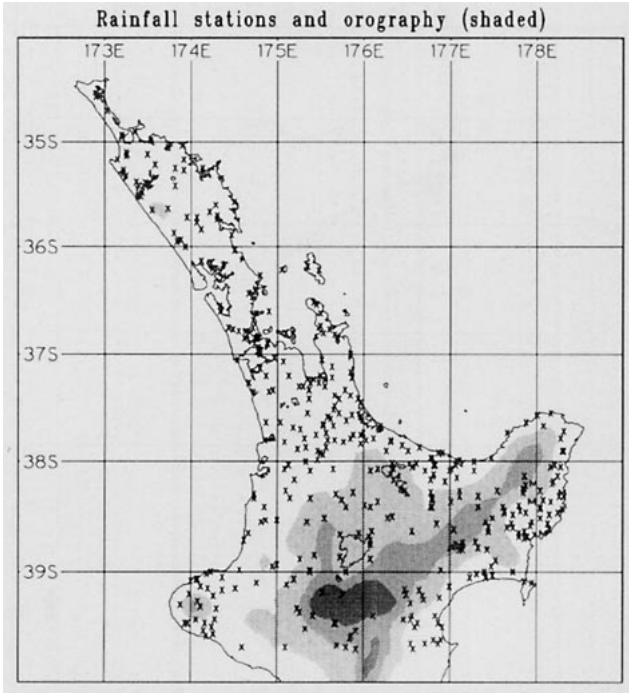

FIG. 2. Rainfall stations (marked with a "×") and topography (shaded). Values between 300 and 600 m—light shading; 600 and 900 m—medium shading; greater than 900 m—heavy shading.

(~10-km) grid, then contoured to produce the daily rainfall maps in Fig. 3. Some experimentation with the analysis scheme was needed to ensure a coherent pattern of rainfall at the expense of smaller-scale variations. A radius of influence of five times the grid spacing was used for the first pass, followed by a second pass with half this radius, followed by a single pass of a 25-point smoother to reduce variability at scales less than twice the grid spacing. It is recognized that such a scheme may arbitrarily blur important details, such as the rain–no rain boundary. Despite this smoothing, it is evident from Fig. 3 that coherent patterns of rainfall variation down to about 50 km are retained.

The contoured rainfall data in Fig. 3 shows that the Gisborne region in the northeast of the NI received the chief impact of the Bola rainstorm. An impressive feature of these maps is that virtually all of this rain fell on the upwind side of the Gisborne Ranges, with heaviest falls during 7 and 8 March. These ranges rise to a maximum height of 1750 m, with much of this barrier above 1000 m. Large areas east of the ranges received daily rainfall totals in excess of 100 mm for two consecutive days, with one location receiving a 419-mm deluge in one 24-h period on 7 March. Another station recorded a storm total of 917 mm. For many locations, the rainfall from Bola represented more than half the annual average. Northland also received storm rainfall totals in excess of 300 mm during this period, with 593 mm at one location.

b. Satellite imagery and surface evolution

Objective data for this study are ECMWF initialized analyses of standard variables on a 2.5° grid at seven standard pressure levels every 12 h. Aspects of the initialization scheme used at ECMWF relevant to vertical velocities and rainfall diagnosis will be briefly discussed in the next section. ECMWF data are supplemented by observational data and IR satellite imagery in order to subjectively establish the realism of the objective analyses before presenting the more detailed diagnostic analysis of following sections.

Satellite imagery is presented in Fig. 4 for each of the four days between 5 and 8 March, during which heavy rain fell over northern New Zealand. Synoptic charts at four corresponding times are presented in Figs. 5 and 6. Figure 5 shows MSL pressure, upper-level relative humidity (RH), and 1000-hPa θ_w as analyzed by ECMWF, along with surface wind and temperature observations. These are used to depict synoptic-scale aspects of the surface evolution of Bola. Comparison of the shaded ECMWF RH fields with the IR satellite imagery enables the realism of the objective humidity analyses to be evaluated, albeit subjectively. Since the IR imagery senses cloud tops, the mean of the 300- and 500-hPa RH was chosen for these comparisons.

The IR imagery for 0200 UTC 5 March (Fig. 4a) shows that any remaining semblance to a TC had vanished. Instead, Bola exhibited the typical asymmetry of an extratropical cyclone, with a broad band of active cloud in the southern semicircle spreading over northern New Zealand. The remains of the front to the south are evident as a weak cloud band extending northwest–southeast across the SI. Both cloud features are realistically resolved by the ECMWF RH field (Fig. 5a), including the "inverted-comma" signature. Despite this asymmetry in Bola's cloud field, 1000-hPa θ_w isopleths still exhibited reasonable concentricity with the MSL pressure field, especially near the core, where values exceeded 20°C. Such warmth near Bola's center is probably residual from its original symmetric hurricane warm-core structure. However, important asymmetries developed later. Most noteworthy of these is the intensifying thermal gradient in Bola's southern sector.

There seems to be reasonable consistency between analyzed θ_w and temperature and dewpoint observations, except on 7 March (Fig. 5c) when analyzed θ_w values near the core were about 2°–3°C warmer than the two nearby ship temperatures. This unfavorable comparison is slightly ameliorated by noting that pressures are below 1000 hPa near the cyclone center. At saturation, the 21°C temperature at the ship near 32.5°S, 175°E (near the center) at a pressure of 978 hPa is equivalent to a θ_w of nearly 22°C.

By 0000 UTC 6 March (Figs. 4 and 5b), the wind, cloud, and rain in Bola's southern semicircle was spreading onto the NI as Bola advanced toward New Zealand. The ECMWF upper-level humidity field re-

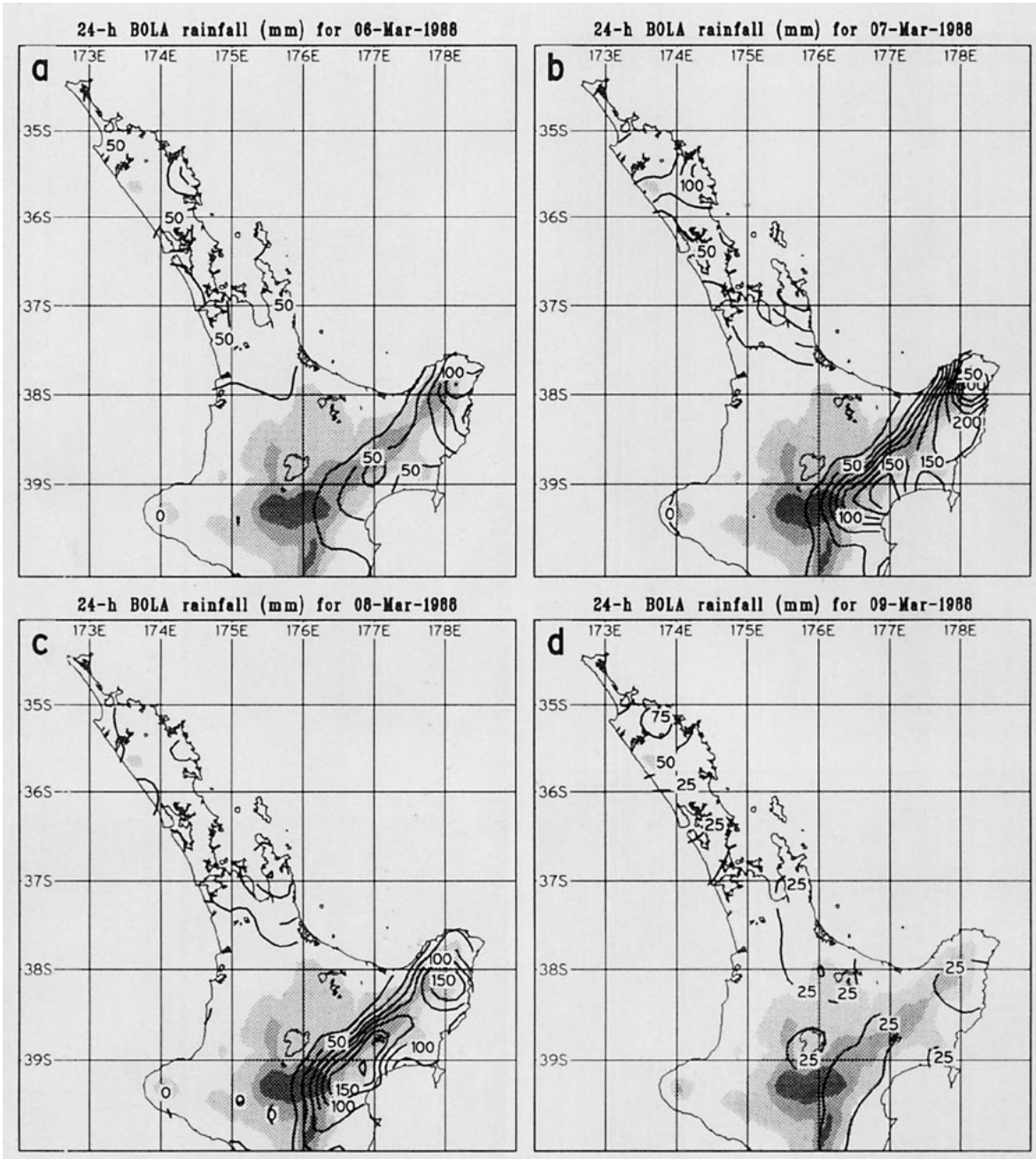

FIG. 3. Rainfall for the 24-h period ending 2000 UTC on (a) 6 March 1988, (b) 7 March 1988, (c) 8 March 1988, and (d) 9 March 1988 as analyzed from the rainfall stations in Fig. 2. Topography shaded as in Fig. 2.

alistically depicted the major cloud features evident in the imagery, including a newly formed cloud band extending northeast from near the low center, and a weak cloud feature in the middle of the Tasman Sea. At about this time, the frontal cloud advancing from the south had merged with the Bola cloud mass. While falling pressures over the NI heralded the approach of Bola from the north, pressures were rising over the SI to the rear of the front. This resulted in a strengthening of easterly flow over the NI.

From about 0000 UTC 7 March, Bola's southward progress was blocked by the intensifying ridge of high pressure to the south. This had the effect of slowing and turning Bola toward the west (Fig. 1). At this time Bola's central pressure was analyzed by ECMWF at 976 hPa. Between Bola and the strengthening ridge to the south, a very strong easterly flow was established over the NI. It was around this time that the heaviest rain fell in Gisborne and Northland (see Fig. 3). As noted earlier, considerable baroclinity was established

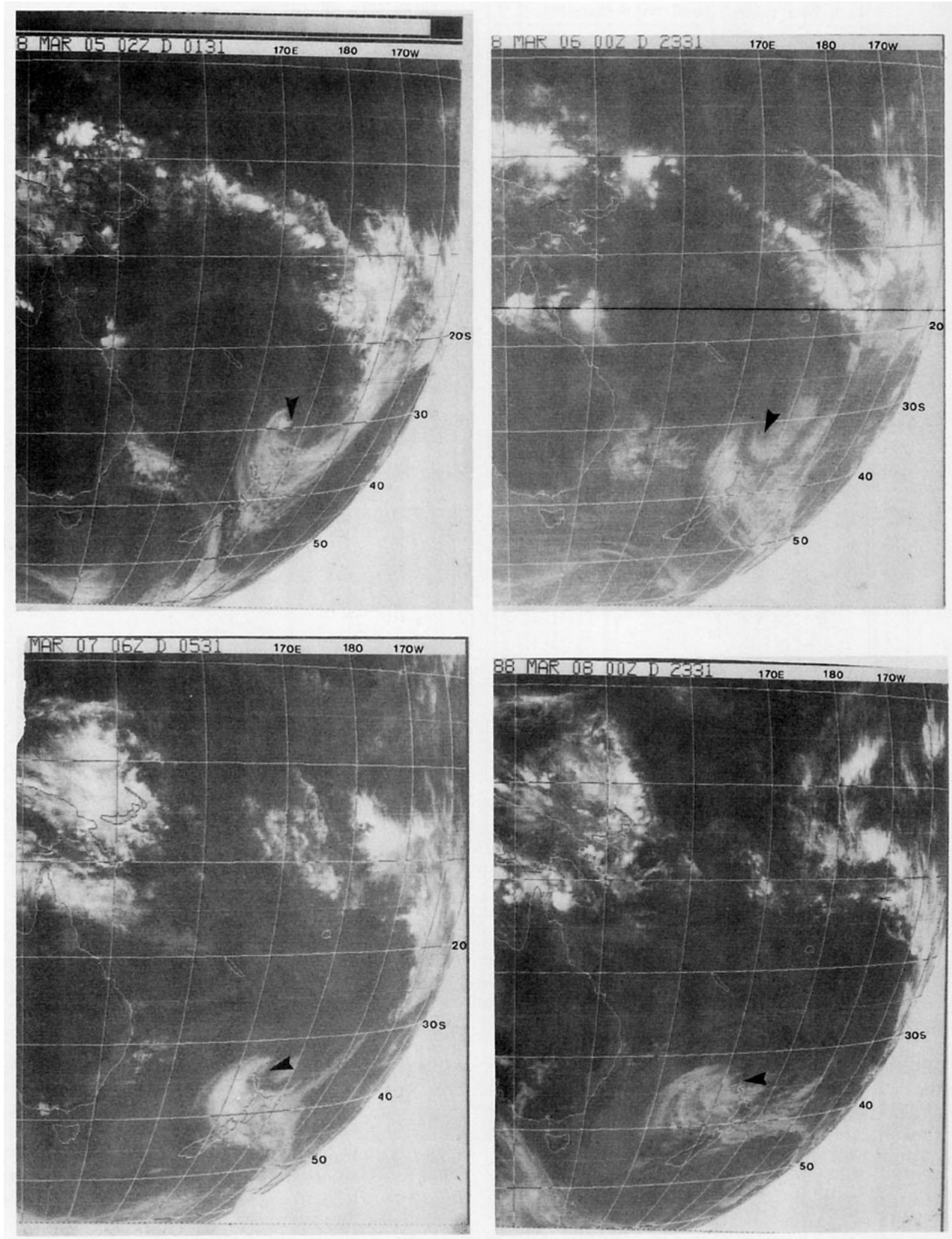

FIG. 4. *GMS-3* low-resolution IR imagery for (a) 0200 UTC 5 March 1988, (b) 0000 UTC 6 March 1988, (c) 0600 UTC 7 March 1988, and (d) 0000 UTC 8 March 1988. The location of the surface center is indicated with an arrow, which also indicates the direction of cyclone motion.

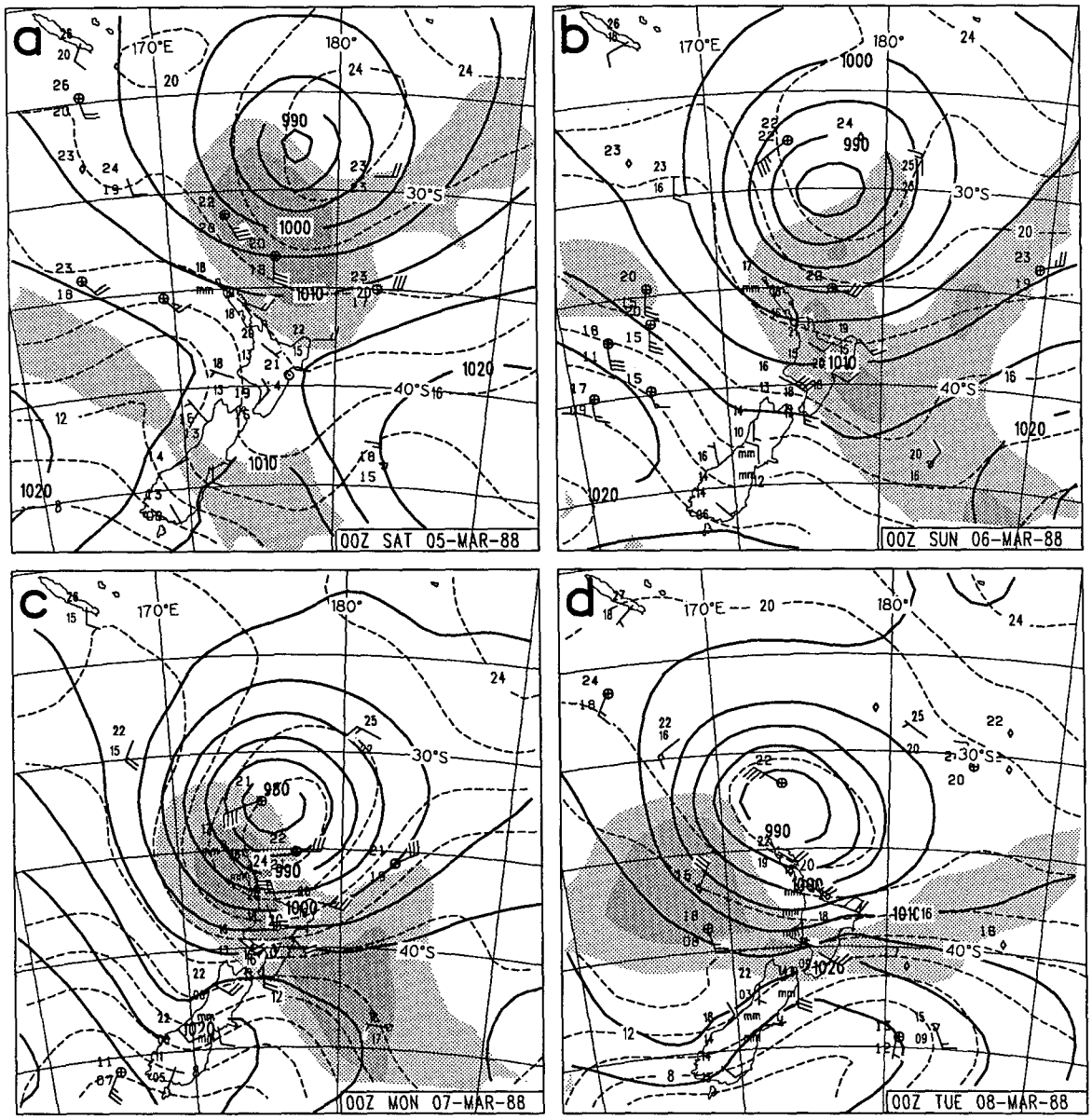

FIG. 5. Selected fields drawn from ECMWF analyses every 24 h as indicated between 0000 UTC 5 March 1988 and 0000 UTC 8 March 1988. Each panel contains mean sea level pressure (solid) every 5 hPa, 1000-hPa θ_w (dashed) every 2°C, and the mean of 500- and 300-hPa RH fields (60%–85%—light shading; >85%—heavy shading), with surface wind observations from land stations, ships (circle enclosing a cross), and drifting buoys (diamond) in knots (1 kt = 0.514 m s^{-1}) with one full (half) barb equal to 10 (5) kt, and one pennant equal to 50 kt.

as warm, moist air flowing around Bola from the northeast merged with cooler, drier air from about the ridge to the southeast. The region of heavy rain in Gisborne occurred more or less within this confluence zone. The role of this confluence and associated frontogenesis will be discussed in section 4. Both the imagery (Fig. 4c) and upper-level RH analysis for this time (Fig. 5c) showed the broad band of cloud covering much of the NI, but with some of the mesoscale detail absent in the objective analyses.

The final panel of the surface maps and the satellite imagery for 0000 UTC 8 March (Figs. 4d and 5d) show some filling of the low and westward translation of the associated cloud features. The most active cloud, now to the west of the NI, extended a band eastward across the lower NI. Later imagery (not shown) showed further westward looping of these ascent areas before Bola finally drifted down the west coast of New Zealand (Fig. 1) and filled slowly before being absorbed into a mobile trough in the westerlies on 12 March. A further

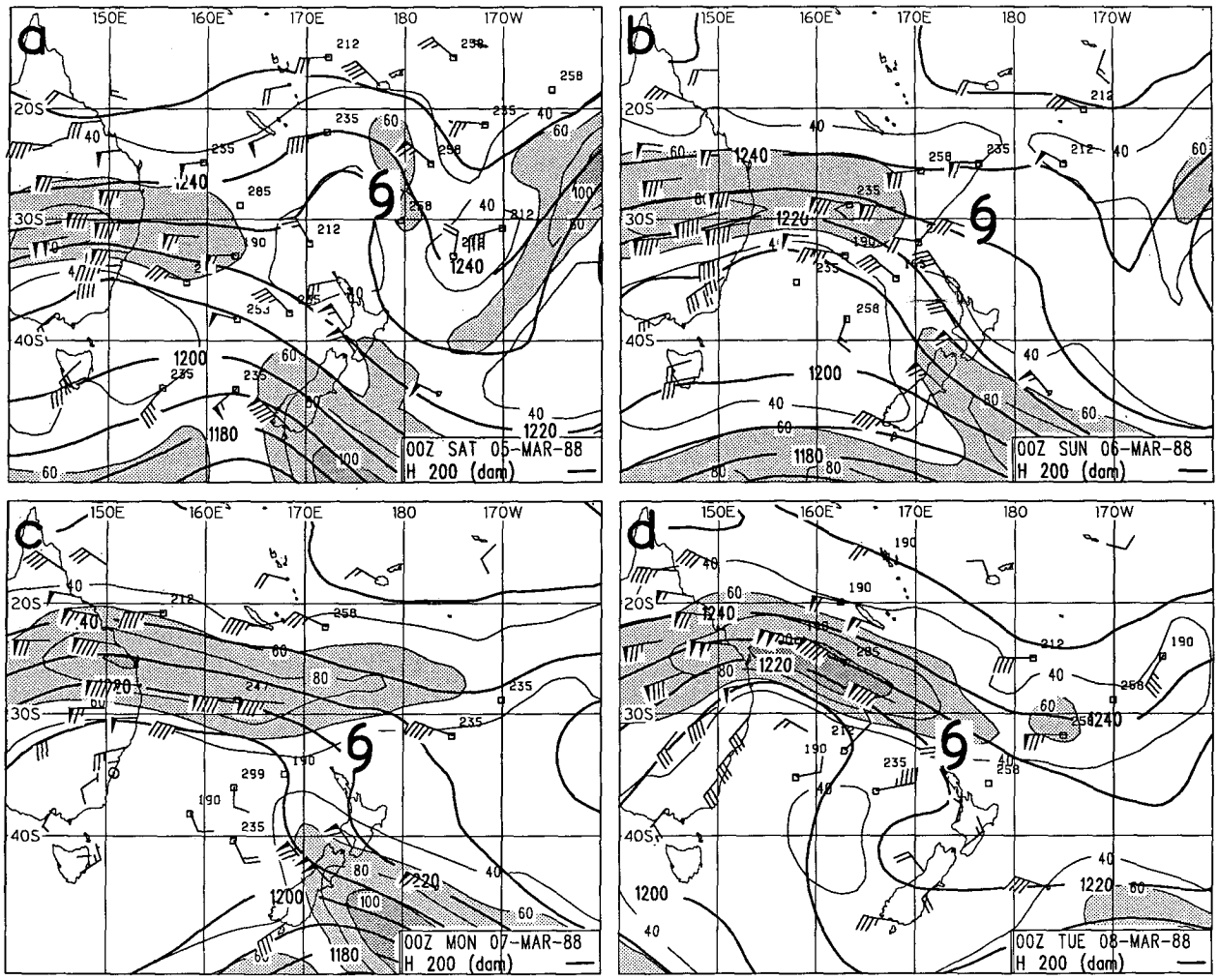

FIG. 6. The 200-hPa height (solid) every 10 dam and isotachs every 20 kt from 60 kt (1 kt = 0.514 m s^{-1}), also shaded (heavy for winds greater than 100 kt) for the four times as for Fig. 5. The position of the surface cyclone center is marked with a hurricane symbol, and rawinsonde and aircraft (annotated with a box) wind observations have been added. Aircraft altitude in hectopascals appears above and to the right.

100–200 mm of rain fell in the north and west of the SI during this final period.

c. 200-hPa features

Aloft, the 200-hPa fields (Fig. 6) at 0000 UTC 5 March (Fig. 6a) reveal cyclonic flow above Bola, with a similar flow at 100 hPa (not shown). Clearly, the characteristic TC anticyclonic upper circulation has been lost at this extratropical stage of Bola's life. The available observations lend credence to the ECMWF objective analyses. Two wind maxima, destined to influence Bola's precipitation, are evident: a subtropical jet (STJ) in the north Tasman Sea approaching from Australia, and another jet streak extending southeast from the SI.

At 0000 UTC 6 March (Fig. 6b), the STJ in the north Tasman was approaching, with deceleration and slightly ageostrophic flow (toward higher heights) near its exit just upstream from Bola. The brightest cloud in the IR imagery for this time (Fig. 4b) just to the west of Northland lay midway between this exit region and the equatorward jet entrance region over the SI. This double jet structure is similar to that observed by DiMego and Bosart (1982a) for Agnes, and is known to favor vigorous tropospheric ascent through interaction of the associated vertical circulations (Uccellini and Kocin 1987). However, although the juxtaposition of the jets appears favorable, ageostrophic flow and acceleration into the SI jet entrance still appear minimal at this stage.

By 7 March (Fig. 6c), the jet entrance over the SI had become quite confluent, with ageostrophic flow toward lower heights and increased wind speeds analyzed in the jet core. This implies an increase in the

vertical circulations about this jet entrance. Maximum cloudiness (Fig. 4c) was contained in the region between the two wind maxima. The role of this distinctive double jet pattern will be discussed in more detail in section 4. The air over the NI was now very anticyclonic, with both curvature and shearing effects contributing.

One day later (Fig. 6d), Bola lay beneath the poleward exit region of the now strengthened STJ in the north Tasman Sea. The wind maximum to the south had receded well to the east by this time. The anticyclonic striations visible in the Tasman Sea cloud near 38°S, 162°E (Fig. 4d) coincided with the sharply turning upper flow in that region.

3. Diagnostic estimation of precipitation

a. Precipitation diagnosis from ECMWF analyses

The chief thrust of this paper is to understand the physical processes associated with the extreme precipitation. In this section, we use standard methods to estimate precipitation rates from Bola using gridpoint data, and compare results with available observations. Since the realism of objectively analyzed fields can be questionable over the SH, it is necessary to first demonstrate that the ECMWF analyses can at least diagnose rainfall at locations where rain actually fell before using the dataset further to analyze related processes.

For several decades, attempts have been made to provide indirect diagnostic estimates of rainfall rates in weather systems using moisture budget methodology on wind and moisture observations (e.g., Bradbury 1957; Palmén 1958; Palmén and Holopainen 1962) or using numerically analyzed datasets (e.g., Smagorinsky and Collins 1955; Carr and Bosart 1978; DiMego and Bosart 1982b). In data-rich regions of the NH, such diagnoses of precipitation have yielded reasonable agreement between the locations of observed and diagnosed rainfall. However, the diagnoses based on objectively analyzed data tended to underestimate observed precipitation, with accuracy generally limited by uncertainty in the analyzed fields and by the substantial variation of observed precipitation over unresolvably small space and time scales.

Diagnostic precipitation estimates from model output of the type described here are critically dependent on how the divergent component of the wind is handled in the analysis and initialization procedures of the model, as noted by Tarbell et al. (1981). Since September 1982, a diabatic nonlinear normal-mode initialization scheme has been in use at ECMWF (Wergen 1987). The introduction of this scheme, and other refinements to the ECMWF model, have contributed to a large increase in the magnitude and realism of analyzed divergent winds and vertical velocities in the tropics (Trenberth and Olsen 1988) that were previously seriously attenuated. In addition, satellite data have had a clear positive impact on ECMWF analyses and forecasts in the SH (Anderssen 1989), suggesting that these data at least partially compensate for the lack of conventional data.

The methodology used here follows Smagorinsky and Collins (1955). Neglecting evaporation, cloud storage, and microphysical processes by simply assuming all condensate immediately falls out as precipitation, the rainfall rate at the surface arising from resolvable saturated adiabatic ascent may be formulated (see Haltiner and Williams 1979, p. 309) as

$$P_s = -\frac{1}{g}\int_0^{P_0} \lambda\delta F\omega\delta p, \qquad (1)$$

where

$$F = \frac{q_s T}{P}\left(\frac{LR - c_p R_v T}{c_p R_v T^2 + q_s L^2}\right),$$

and $\delta = 1$ for $\omega < 0$; 0 otherwise, and $\lambda = [(q/q_s) - 0.6]/0.4$ for $q/q_s > 0.6$; 0 otherwise.

The parameterization of the coefficient λ arbitrarily assumes that condensation begins at 60% saturation, as suggested by Haltiner and Williams (1979).

The diagnostic rainfall rate estimates (Fig. 7) based on (1) over 2 days of the most intense rain yield precipitation over and to the north of the NI. Subjectively, these precipitation patterns are similar to the regions of maximum cloudiness in the satellite imagery in Fig. 4. Maximum instantaneous rates exceeding 2 mm h^{-1} (48 mm day^{-1}) occur just east of Northland at 1200 UTC 7 March. Figure 8 is the result when (1) is summed for the 10 times every 12 h between 0000 UTC 5 March and 1200 UTC 9 March and converted to a rainfall total. In the Gisborne region, 5-day totals of 50–60 mm are diagnosed, with 60–80 mm over Northland. Apart from analysis uncertainty, the validity of such totals obtained from 12-h analyses is also questionable in view of the large differences in the instantaneous rates from one time to the next.

Figure 9 shows observed 5-day storm rainfall totals contoured as for Fig. 3 over regions where rainfall observations are available. It is immediately clear that the large rainfall amounts on the eastern slopes of the Gisborne ranges in Fig. 9 were not obtained by the diagnostic calculation in Fig. 8. Nevertheless, rainfall totals of between 20 and 60 mm *west* of the Gisborne Ranges were closer to the diagnosed values in Fig. 8, although they were experienced in a region sheltered from the east. Listings from individual stations for low-lying regions near Auckland City (36.9°S, 174.8°E) better exposed to the east revealed higher totals of between 120 and 190 mm, averaging 145 mm for 25 stations within a 50-km radius of Auckland. Many of the values near the higher end of this range were recorded over or near higher ground (up to 300-m elevation).

In summary, this attempt to establish the accuracy of the precipitation rate diagnoses by comparison with rainfall observations is only quantitatively possible for

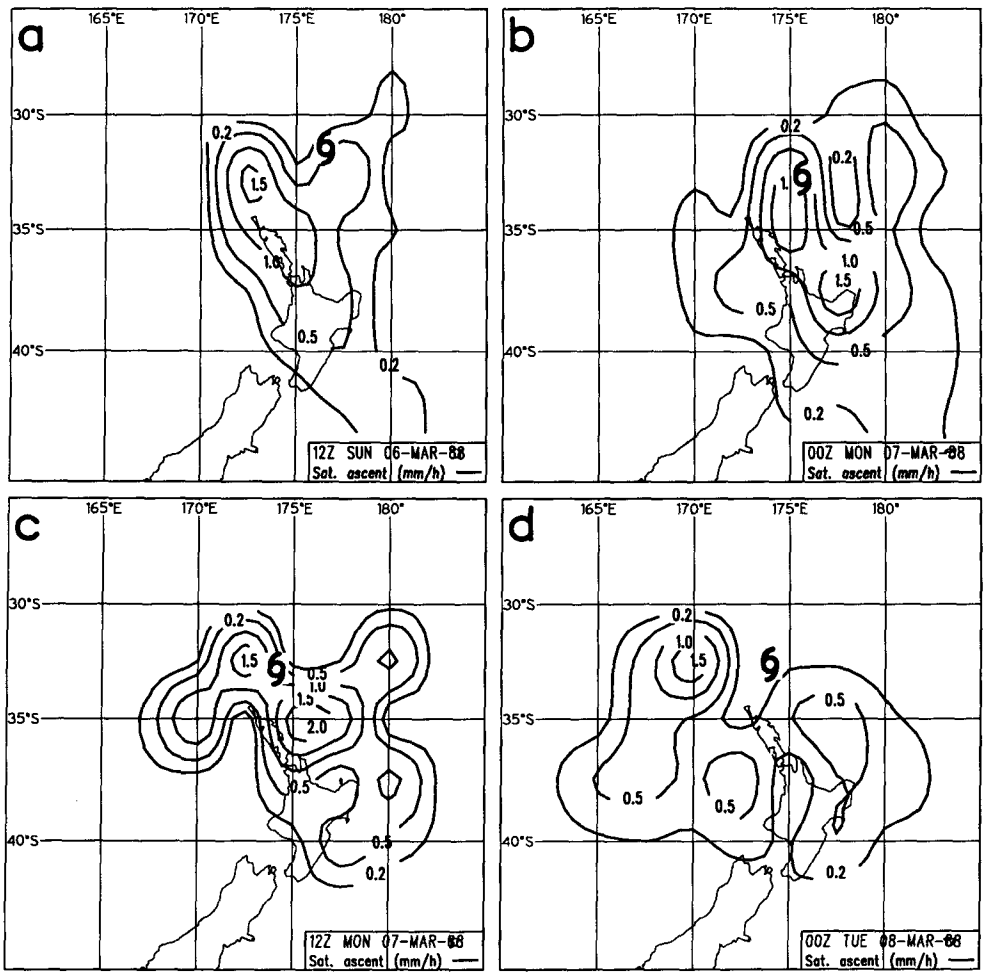

FIG. 7. Diagnostic estimates of precipitation rates drawn every 0.5 mm h^{-1} for the four times between 1200 UTC 6 March and 0000 UTC 8 March. The 0.2 mm h^{-1} contour is added. The cyclone position is indicated.

a very small fraction of the storm domain and is greatly complicated by the high dependence of rainfall on terrain. Overall, the diagnostic estimates of Figs. 7 and 8 appear to capture the broad regions of precipitation expected on the basis of satellite imagery, but fall short of observed rainfall (Fig. 9), especially on the upwind side of mountains. Away from the mountains, better agreement is obtained, although the diagnoses still tend to underestimate observed rainfall in places exposed to Bola's easterlies.

b. *Orographic precipitation*

To gain some insight into the failure of the precipitation calculations to capture the large rainfall amounts over the Gisborne Ranges, we examined vertical p velocity (ω) fields from the ECMWF dataset (Fig. 10) in relation to the NI terrain. These generally resemble the precipitation rates in Fig. 7, not surprisingly, since (1) is a weighted vertical integral of ω through the atmosphere. At 850 hPa (Figs. 10i–l), there is a persistent ascent–descent dipole over the NI comprising ascent (descent) east (west) of the NI, also present at reduced amplitude at 700 hPa (Figs. 10e–h). This dipole is suggestive of the pattern of ascent expected for easterly flow over elevated NI terrain. To confirm this, we computed the orographically forced vertical motion

$$\omega_s \sim -\rho_0 g \mathbf{V}_s \cdot \nabla h, \tag{2}$$

where h is the terrain height and $\mathbf{V}_s$ is a representative surface-layer wind velocity, estimated here as the average of $\mathbf{V}$ at 850 and 1000 hPa as analyzed at 0000 UTC 7 March. The actual ECMWF orography was not available for this calculation. However, the T106 spectral resolution used by ECMWF during 1988 would probably resolve topography details down to about 100 km. Accordingly, New Zealand topography (available to 500-m horizontal resolution), averaged onto a

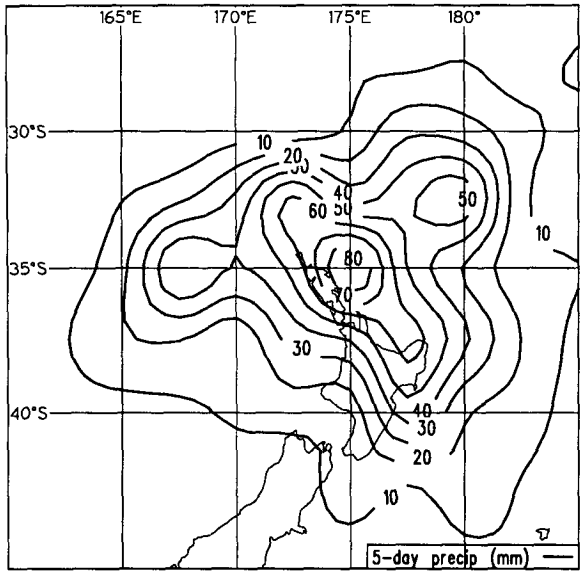

FIG. 8. Five-day diagnostic precipitation totals drawn every 0.5 mm h^{-1} for the period 0000 UTC 5 March–1200 UTC 9 March.

100-km grid (Fig. 11a), was used to compute orographic vertical-motion patterns (Fig. 11b) using (2). These were found to exhibit a dipole of similar magnitude to that in Fig. 10f. Naturally, at such coarse resolution, the shape of the orographic features and their related vertical-motion patterns depends on the exact placement of the grid points. Nevertheless, it is apparent that both the magnitude and location of the dipoles in Fig. 10 over the NI are consistent with their generation by flow over terrain similar to that in Fig. 11a. The importance of this topographic component in relation to the overall ascent fields in Fig. 10 and to the resulting precipitation diagnoses in Figs. 7 and 8 is still, however, fairly small.

This simple calculation suggests that the coarse depiction of the ECMWF orography is the primary reason for the underdiagnosis of orographic precipitation. To determine the likely impact of higher-resolution topography, ω_s was computed from (2) on a 10-km grid. The topography at this higher resolution (Fig. 11c) better depicts the mountains west of Gisborne and other NI features. The calculation of ω_s yielded a dipole (Fig. 11d) almost an order of magnitude larger than that computed for the 100-km grid (Fig. 11b). Orographic precipitation was computed using (1) by assuming that the uplift in Fig. 11d applied throughout the atmospheric column below 300 hPa. Ascent along the saturated adiabat defined by the ECMWF 1000-hPa T and RH was assumed. On the 10-km grid used for this calculation, downwind drift of hydrometeors becomes important. Rain was assumed to fall at 7 m s^{-1}, while snow (above the freezing level) fell at 1 m s^{-1}. This drift slightly spreads resulting surface accumulations downwind (i.e., over the mountain crest). In recognition of the fact that abundant moisture is needed for precipitation, results were multiplied by a factor $(RH_{850} - 0.8)/0.2$, with zero precipitation for RH_{850} less than 0.8 (80% saturation). This reduced precipitation over mountains to the west of the Gisborne Ranges where only 85%–90% saturation was analyzed by the large-scale ECMWF analyses.

The resulting computed precipitation rates at the surface (Fig. 11e) are in good quantitative and qualitative agreement with the observed 24-h rainfall totals (Fig. 11f). This huge improvement over the estimates in Fig. 7 is a consequence of using the more detailed topography in Fig. 11c to resolve the topographic gradients responsible for the large upslope rainfall (Fig. 11f). The horizontal distribution of diagnosed precipitation in Fig. 11e is determined by the terrain-induced ascent (Fig. 11d), but with slight spreading downwind as described earlier. However, the *magnitude* of the resulting patterns is dependent on how ω_s (or the slope of the streamlines) varies with height. By judicious choice of ω profile, we were able to make the patterns agree in magnitude with observed rainfall. The assumptions here that the vertical velocities occur throughout a vertical column directly above the mountain slope and that all the computed condensed water falls out are probably optimal for maximizing the resulting precipitation. Sawyer (1956) found similar agreement between observed rainfall and total computed condensed water only for cases where deep moisture was available for orographic precipitation.

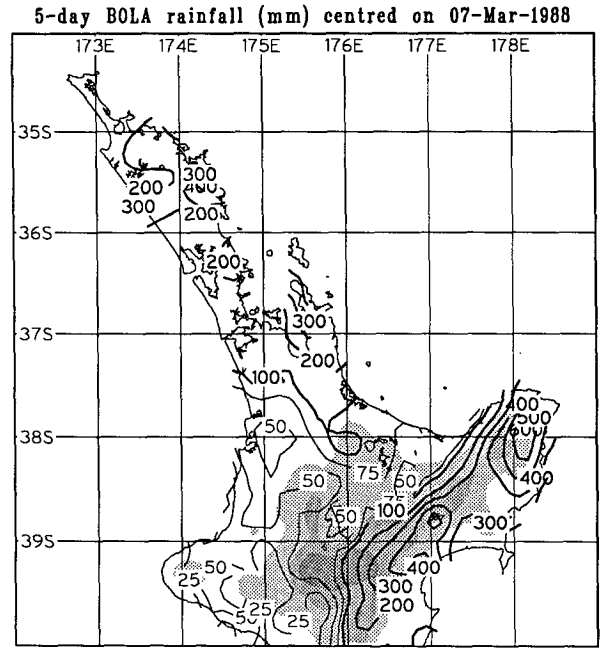

FIG. 9. Five-day observed rainfall totals contoured as in Fig. 3 from the rainfall stations in Fig. 2. Contours are every 100 mm, except in the range 0–100 mm where lighter contours are every 25 mm.

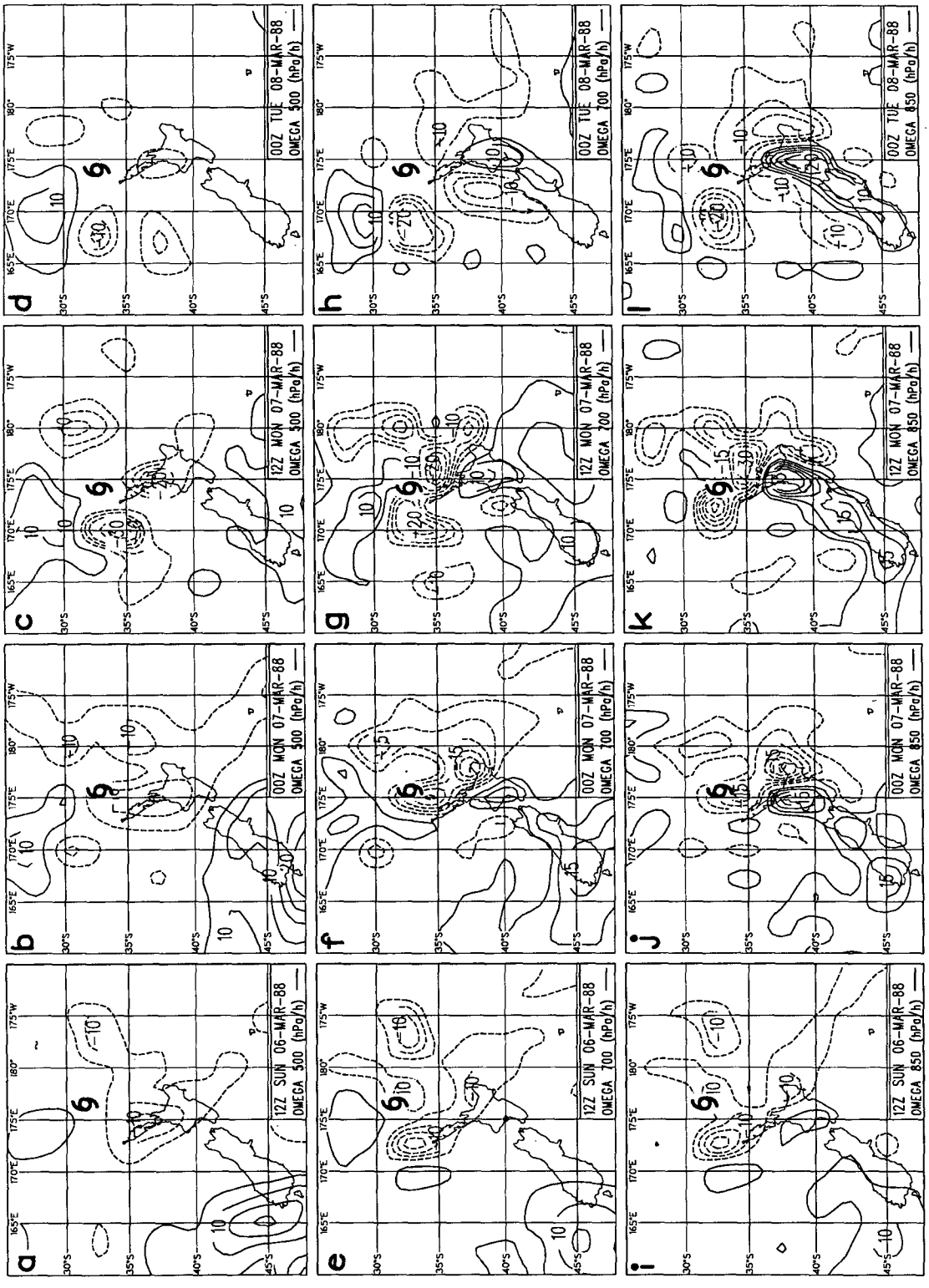

FIG. 10. Vertical p velocity fields every 12 h between 1200 UTC 6 March and 0000 UTC 8 March at (a)–(d) 500 hPa, (e)–(h) 700 hPa, and (i)–(l) 850 hPa, drawn every 5 hPa h^{-1}, with positive (negative) contour values solid (dashed) and the zero contour omitted for clarity. The cyclone position is marked.

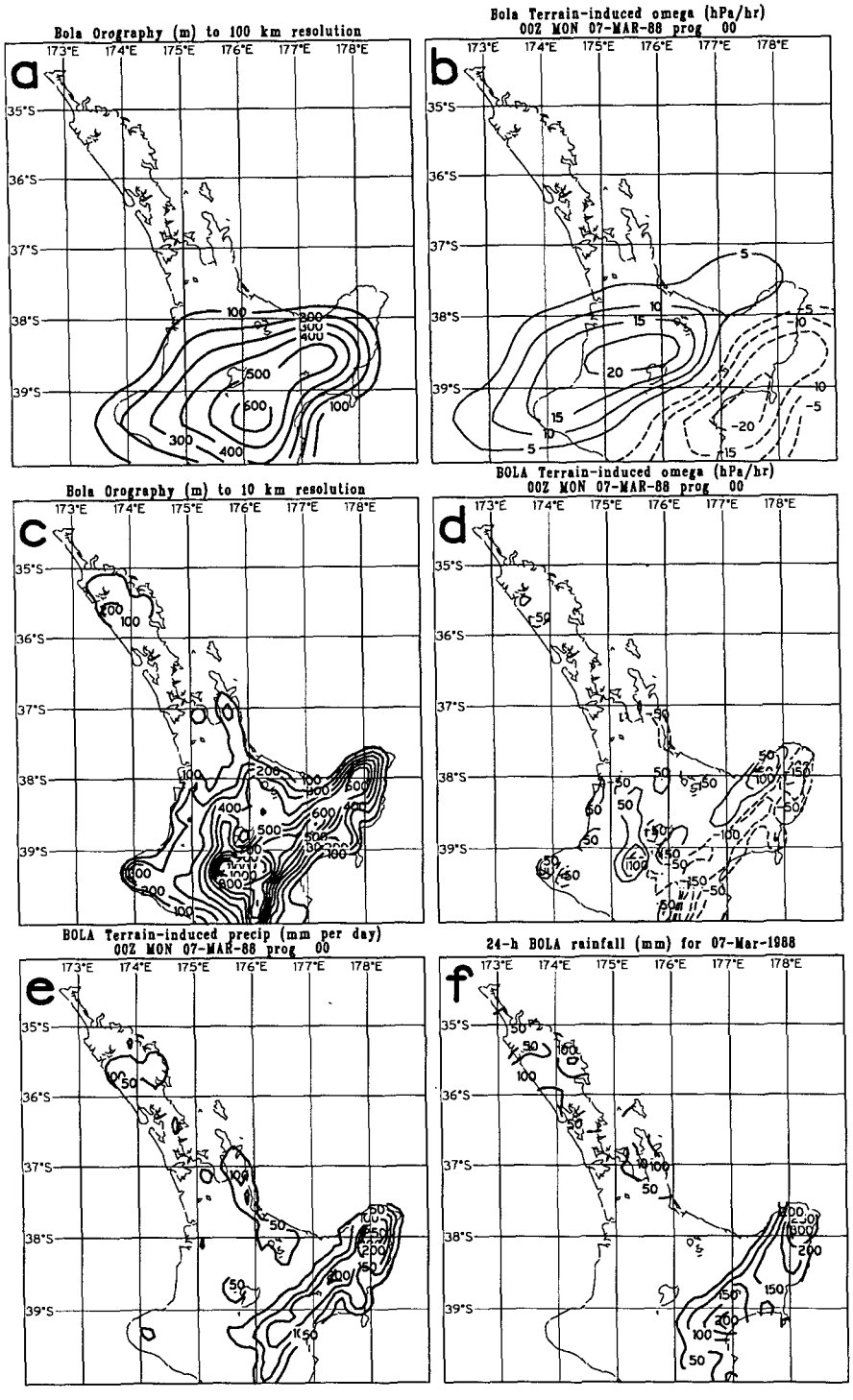

FIG. 11. (a) North Island orography at 100-km resolution, contours every 100 m; (b) terrain-induced ω every 5 hPa h^{-1} computed using the terrain in (a), with positive (negative) contour values solid (dashed) and the zero contour solid; (c) orography at 10-km resolution every 100 m; (d) terrain-induced ω every 50 hPa h^{-1} computed using the terrain in (c); (e) orographic precipitation for 0000 UTC 7 March every 50 mm day^{-1}; and (f) as for (e) except 24-h rainfall.

The spurious regions of precipitation in Fig. 11e about hills to the west of the main Gisborne Ranges would probably be eliminated by the inclusion of lee warming and drying effects in the calculation. Another discrepancy between the two patterns is that the observed rainfall extends farther upwind (toward the coast) than diagnosed. This may be because some of the lifting aloft begins upstream from the mountains (e.g., Queney 1948), possibly compounded by the associated release of convective instability. The reader is referred to Smith (1979) for a fuller discussion of the issues associated with orographic precipitation.

We conclude that the rainfall over Gisborne from Tropical Cyclone Bola was largely determined by the local topography as warm, moist air ascended the mountain ranges. The simple calculation of orographic ascent presented here was able to realistically replicate the observed rainfall variations when details of the topography down to 10 km were used. Although mesoscale models provide the most complete specification of the complex interacting processes associated with orographic precipitation, the simple scheme described here appears to give realistic results, despite neglect of important processes. Quantitatively, these diagnoses depend on the specification of an ω profile and on grid resolution. Such a scheme may have some utility in estimating the rainfall in relation to the topography when initialized with surface wind, temperature, and moisture forecasts from a large-scale model for an expected heavy-rain event. Since observed rainfall frequently exhibits a well-defined relation to topography, the scheme may also be used to provide meaningful interpolation between sparse raingage data.

4. Dynamic and thermodynamic analysis

In the previous section, it was shown that estimates of precipitation based on the ECMWF analyses were able to reproduce the broad features of the precipitation field of cyclone Bola. However, the resulting patterns lacked mesoscale detail, and in particular, the large rainfall amounts on the upslope side of the Gisborne Ranges and in Northland were underestimated. Nevertheless, since the ECMWF analyses were able to diagnose ascent at locations where rain actually fell, an examination of the dynamical and thermodynamic processes responsible for the larger-scale ascent is warranted.

a. Quasigeostrophic diagnosis

According to quasigeostrophic (QG) theory, ascent is associated with an increase with height of cyclonic vorticity advection (CVA) and warm advection, and it is augmented by latent heat release in the ascending air. The relative importance of these factors is investigated (Fig. 12) during the period of heaviest rain.

At 300 hPa, a region of strong CVA and divergence (shaded) is located downstream from the upper trough associated with Bola (Figs. 12a–c). In Fig. 12a, the tongue of cyclonic vorticity along 30°S coincides with the cyclonic shear side of the approaching upper wind maximum (Figs. 6b,c). Intensification of the Bola upper cyclonic vorticity maximum (Fig. 12b) appears to coincide with the approach of this STJ to the north. At the same time, there is increasing anticyclonic shear along the equatorward flank of the strengthening jet entrance over the SI. This contributes to an increase in the anticyclonicity of the ridge over the NI. Between the two, a substantial vorticity gradient develops about and to the north of the NI (Figs. 12b,c). Thus, the CVA about and to the north of the NI appears linked to the distinctive double jet signature evident in Fig. 6.

Although CVA seems to maximize between the upper trough and the downstream ridge, the divergence in Fig. 12 tends to be strongest nearer the ridge, since the vorticity equation requires more divergence to balance CVA in a low absolute vorticity environment. This is especially true if there is, in addition, an anticyclonic tendency of vorticity within the ridge such as is apparent between Figs. 12a and 12b.

Thermal advection can be inferred from Figs. 12d–f. Warm advection is apparent at 700 hPa in the region east of the NI. This is augmented by apparent frontogenesis to the south of Bola and by the increase in circulation apparent between the first two times.

The QG omega equation

$$\left(\nabla^2 + \frac{f_0^2}{\sigma}\frac{\partial^2}{\partial p^2}\right)\omega = \frac{f_0}{\sigma}\frac{\partial}{\partial p}\left[\mathbf{V}_g\cdot\nabla\left(\frac{1}{f_0}\nabla^2\Phi + f\right)\right] + \frac{1}{\sigma}\nabla^2\left[\mathbf{V}_g\cdot\nabla\left(-\frac{\partial\Phi}{\partial p}\right)\right] \quad (3)$$

is used to compute the vertical p velocity resulting from a vertical gradient of geostrophic vorticity advection and the Laplacian of geostrophic thermal advection. Additional contributions to vertical motion arising from diabatic effects, friction, the divergent part of the wind, and other terms in the vorticity equation are neglected in this simple QG formulation. The neglect of the horizontal variation of static stability, σ [here, $\sigma = \sigma(P)$ from standard atmosphere] is also a source of error (Danard 1964). Sequential overrelaxation with $\omega = 0$ at 100 and 1000 hPa was used to solve (3).

The QG ω patterns in Figs. 12g–i depict a general region of ascent to the east and northeast of the NI but miss some of the features of the full model ω patterns in Fig. 10. In particular, the distinctive inverted-comma ascent signature at 0000 UTC 7 March is absent, although QG ascent does maximize at this time, which corresponds to the period of heaviest rainfall (see Fig. 3). Descent is evident to the northwest of the Bola center.

Next, the relative importance of the two forcings included in (3) was determined by solving the omega equation with each of these in turn as a single forcing

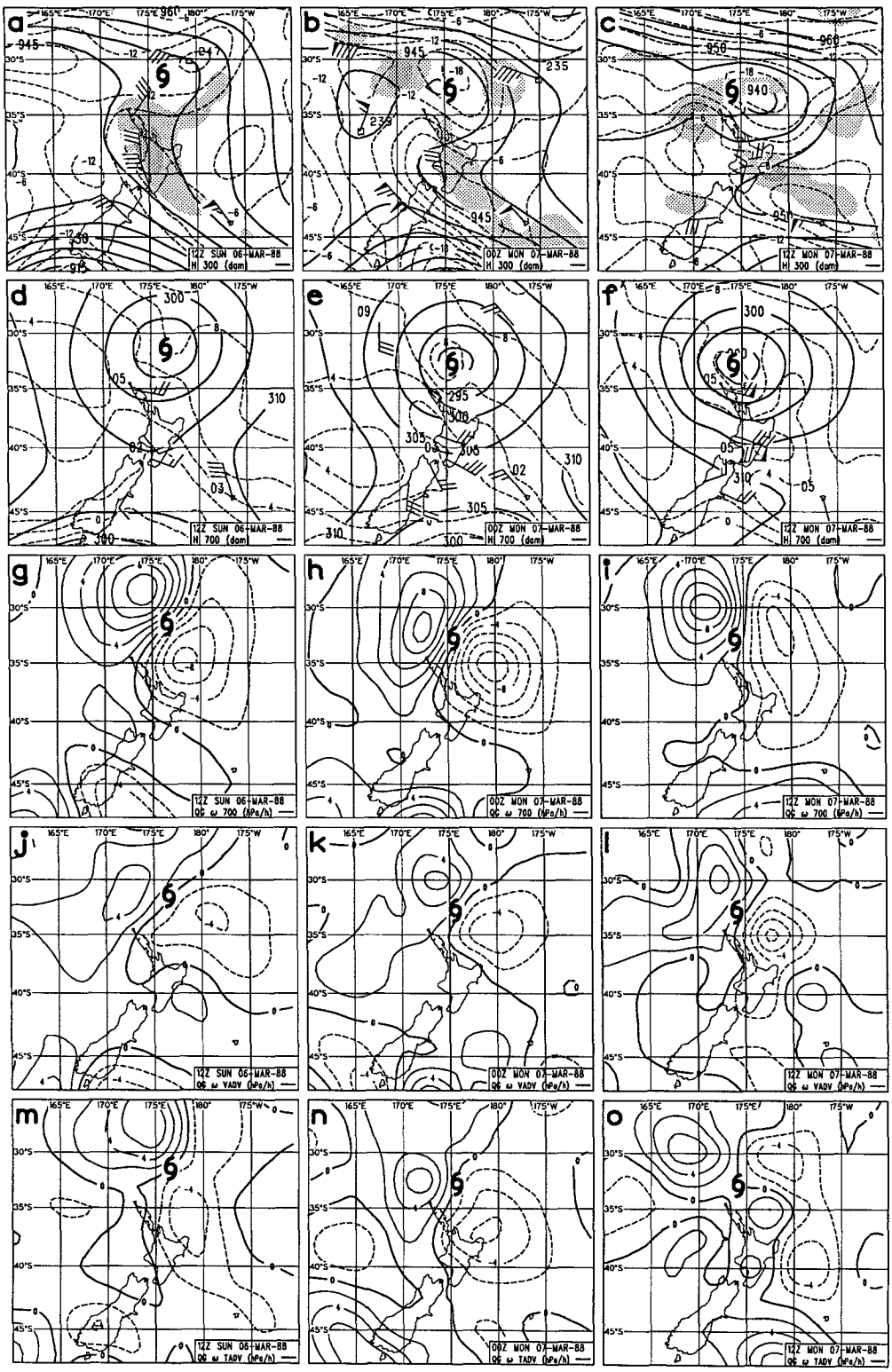

FIG. 12. Selected fields every 12 h between 1200 UTC 6 March and 1200 UTC 7 March: (a)–(d) 300-hPa height (solid) every 5 dam, ζ_a (dashed) every 3×10^{-5} s^{-1} and $\nabla \cdot \mathbf{V}$ shaded (light shading between 10 and 20×10^{-6} s^{-1} and heavy greater than 20×10^{-6} s^{-1}), plus wind observations as in Fig. 6; (d)–(f) 700-hPa height (solid) every 5 dam and temperature (dashed) every 2°C, with wind and temperature observations added; (g)–(i) QG ω every 2 hPa h^{-1}; (j)–(l) as for (g)–(i) except with just vorticity advection forcing; and (m)–(o) as for (g)–(i) except just thermal advection forcing. Contouring convention for (g)–(o) as for Fig. 11b.

on the right-hand side of (3). It is beyond the scope of this paper to more completely partition the full model ω fields (see DiMego and Bosart 1982a). Since condensational heating is related to the rate of ascent, its contribution, although not computed directly, would be expected to resemble (and hence, augment) the total ascent (Figs. 12g–i).

The results of the simple partitioning here into vorticity and thermal advection components are consistent with the first two rows of Fig. 12 discussed earlier. The vertical derivative of geostrophic vorticity advection (Figs. 12j–l) yielded ascent to the northeast of the NI, in the general region of upper-level CVA as inferred from Figs. 12a–c. Thermal advection tended to maximize a little to the south of the CVA, with its Laplacian forcing ascent about and to the east of the Gisborne region (Figs. 12m–o).

Hoskins et al. (1978) warn that consideration of these terms in isolation is misleading since there is a degree of cancellation between them. This is because each term contains the identical component $f\mathbf{V}_g \cdot \nabla(\partial\zeta_g/\partial z)$ with opposite sign (so they cancel when the two are summed), which is not "Galilian invariant." In view of this tendency to cancel, the fact that these two components actually reinforce in the region northeast of the NI during the first two times is noteworthy. This overlap is especially apparent at 0000 UTC 7 March when the heaviest rain fell. A similar in-phase relationship between these two terms was noted by DiMego and Bosart (1982a) in association with the Agnes rainstorm. This QG analysis finds that the Bola ascent can be explained by superposition of an area of appreciable upper-level vorticity advection over an area of increasing low-level thermal advection, combined with additional diabatic forcing. These three factors will now be examined in relation to surrounding synoptic features.

b. *Relationships with jet-streak circulations*

The 200-hPa charts (Fig. 6) described in section 2 revealed that ascent largely occurred in the region between the poleward exit region of the westerly STJ to the north of Bola and the confluent entrance to the second jet southeast of the SI. The associated vorticity patterns make this an area of substantial CVA, as already noted. Such a double upper-jet configuration is a classic heavy-rain signature in any part of the world (e.g., Uccellini and Kocin 1987).

A cross section (Fig. 13) is used to examine the vertical circulations associated with the two jet streaks in Fig. 6c. This great-circle vertical section extends from near the axis of the southern jet, through the ascent zone near Gisborne, over the center of Bola, and then through the STJ to the north. The two jets are directed out of the page in Fig. 13. Two jet-related vertical circulation features sharing the same ascent branch are evident. About the confluent jet entrance over the SI

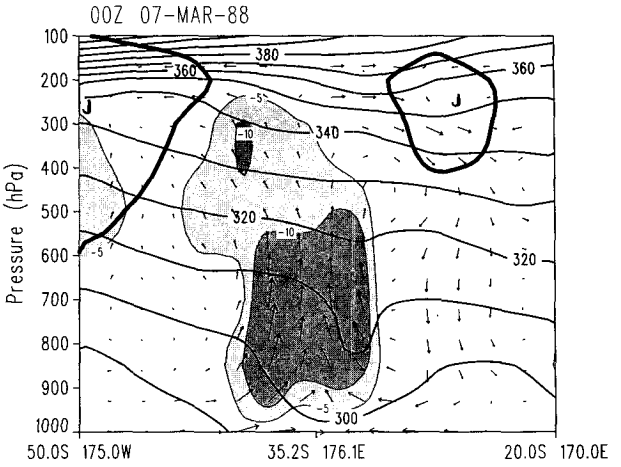

FIG. 13. Cross section along indicated great-circle line for 0000 UTC 7 March. Potential temperature (solid) every 10 K, ascent less than -5 (-10) hPa h^{-1} light (heavy) shading, and the 60-kt (30.8 m s^{-1}) contour of wind speed (thick). Vectors represent ageostrophic wind components in the plane of the section and vertical motions, scaled in the ratio 1:10, where one horizontal (vertical) grid spacing represents 6 (0.6) m s^{-1}.

(left side of Fig. 13), there is a thermally direct circulation comprising ascent beneath the equatorward flank of this jet and ageostrophic flow directed toward lower pressure (see Fig. 6c) into the jet aloft. The second circulation cell about the STJ is indirect, with ageostrophic motion aloft toward higher pressure. Above the ascent, divergent ageostrophic flow occurs between the upper branches of these two circulations.

This double jet pattern and associated two-cell vertical circulation pattern is similar to that described by Uccellini and Kocin (1987) in association with heavy snow events over the eastern United States. However, a significant ridge developed between the two jets (see Fig. 6) that was not observed in the NH winter cases. This upper ridge is possibly a consequence of the increased significance of condensational heating here, as the Bola ascent occurred within a moist, subtropical air mass. The strong low-level warm anomaly in Fig. 13 associated with the cyclone core is another unique feature of the present case. It is left over from the previous warm-core hurricane structure.

In describing the relationship with these upper-jet features, we have been careful to avoid discussion of cause and effect. The massive heating associated with tropical cyclone remnants entering middle latitudes is known to export considerable kinetic energy into the downstream jet entrance (Palmén 1958). Sinclair (1992) noted that a small downstream upper jet streak associated with the remnants of Tropical Cyclone Patsy appeared to be "locked onto" the poleward-moving cyclone. In that case the association was probably cooperative, with the entrance region providing a favorable upper-level environment for ascent while the jet was in turn sustained by the outflow from the diabat-

ically enhanced ascent. In the case of Bola, the SI jet was a preexisting feature associated with a weak (as far as ascent is concerned) cold front. The subsequent interaction that occurred as the distance between the STJ and the SI jet closed appeared to invigorate the downstream jet and the associated ageostrophic motions.

It is noteworthy that previous tropical cyclone remnants causing severe weather over New Zealand also became coupled with the equatorward entrance regions of preexisting upper-level jets. New Zealand's most lethal storm this century, Tropical Cyclone Giselle (Hill 1970), intensified beneath the equatorward entrance region of a jet extending southeastward from central New Zealand, while Tropical Cyclone Norman (Trenberth 1977) had an upper-air configuration not unlike that described here for Bola. Examination of several further cases is needed to confirm that such a configuration is a general feature accompanying regeneration of tropical cyclone remnants in the New Zealand area.

c. *Low-level processes*

In accounting for the rain associated with Bola, we need to also examine processes at lower levels of the atmosphere. Strong ascent and an abundant moisture supply at low levels are necessary ingredients for heavy precipitation. The northeast flow about Bola's eastern flank is a source of moisture-rich tropical air. This meets cooler air from around the ridge to the south in a confluent region about and to the east of the NI, as described in section 2 (see Fig. 5).

Low-level confluence has several interrelated roles. First, a confluent axis oriented at a small angle to the isotherms is frontogenetic, with potential for enhanced warm advection contributing to ascent. Second, the frontogenetic vertical circulations can contribute to the ascent field. Finally (and importantly), any associated moisture convergence acts as a low-level moisture source for precipitation.

These aspects of the confluence are examined for 0000 UTC 7 March with the aid of Fig. 14. Low-level moisture convergence $\nabla \cdot q\mathbf{V}$ (shaded) was computed from the ECMWF data; 850 hPa was used for this calculation, since the 1000-hPa results were overwhelmingly dominated by inflow at the center of Bola. Results show that the confluence supports a small region of moisture convergence east of Gisborne. This is upwind from the local maximum of low-level ascent (Figs. 10f, j) over Gisborne at this time. Stronger moisture convergence was also located near Northland, better correlated with the ascent there.

Locally stronger moisture convergence not resolved by the ECMWF data undoubtedly existed closer to the upwind side of the Gisborne ranges, as required to "feed" the large precipitation observed there. Lack of wind data prevented any independent mesoscale assessment of low-level convergence. However, surface wind observations along the Gisborne coast additional

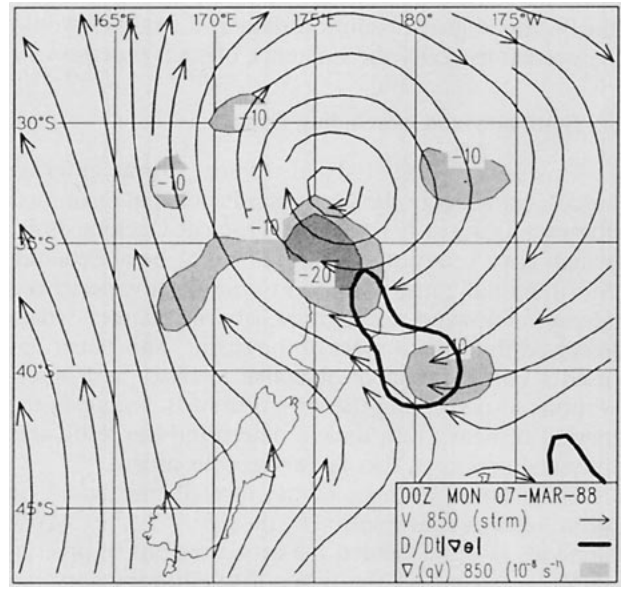

FIG. 14. The 850-hPa streamlines, $\nabla \cdot q\mathbf{V}$ ($<-10 \times 10^{-8}$ s^{-1}—light shading, $<-20 \times 10^{-8}$ s^{-1}—heavy shading), and the 3×10^{-10} °C m^{-1} s^{-1} contour of frontogenesis (thick) for 0000 UTC 7 March.

to those included in Fig. 5c were from the southeast, that is, about 45° across the isobars toward lower pressure. It is possible that the damming influence of the Gisborne ranges would contribute to this southerly component. In contrast, wind over open water to the northeast of Gisborne (see the ship in Fig. 5c) blew at an angle of only 20° to the isobars.

Figure 14 also shows that this confluent region was frontogenetic near Gisborne. Frontogenesis was computed using the Petterssen (1956, p. 202) formula based on actual (ECMWF) winds. It is tempting to speculate that the larger-scale ascent was locally enhanced in this region by the vertical circulation associated with this frontogenesis. Bosart and Dean (1991) noted that the heaviest Agnes rainfall occurred near a mesoscale frontal boundary embedded within a larger-scale ascent region, with frontogenesis assisted by the ageostrophic downgradient flow channeled by the Appalachian Mountains on the cooler side of the front. Unfortunately, lack of detailed observations precludes any similar definitive mesoscale analysis over the Gisborne region.

In summary, low-level processes conducive to ascent and precipitation were observed to the east of the NI. These included frontogenesis and modest moisture convergence where warm, moist northeasterly flow met the cooler southeasterly flow to the east of the NI. Although this confluence was not exactly collocated with the strongest low-level ascent diagnosed by the ECMWF model, it is suggested that the frontogenetic forcing may, in reality, be locally enhanced nearer the ranges, contributing to a local focusing of ascent near

Gisborne. Higher-resolution data and analyses would be needed to verify the existence of such processes.

5. Summary and concluding remarks

This second case study of tropical storms entering middle latitudes in the southwest Pacific has examined the extratropical behavior of Tropical Cyclone Bola, which gave heavy rain to the north of New Zealand. Storm rainfall totals of up to 917 mm were experienced along the upwind side of the Gisborne Ranges, which received the chief impact of the storm. This paper has used a combination of objective analyses and observations to determine the structure of Bola during the period of heavy rain and to determine the resolvable physical processes that favor vigorous ascent.

Diagnostic estimates of the rainfall rate based on saturated ascent as resolved by the 2.5° × 2.5° ECMWF analyses (Fig. 8) yielded the broad regions of precipitation expected on the basis of satellite imagery but underestimated the huge rainfall totals (Fig. 9) observed on the upwind side of mountains. Quantitative agreement was better away from the mountains. A wider comparison with rainfall observations was thwarted by an absence of rainfall data over the oceans. Lack of model resolution was the main reason for the failure of these coarse diagnoses to resolve the substantial and detailed orographic component of observed rainfall over New Zealand.

In view of the observed link between rainfall and topography, a simple scheme to compute the important orographic component of precipitation was formulated. This was based on ascent induced by flow over the mountains. Results in good agreement with 24-h rainfall totals were obtained when the terrain was resolved to approximately 10 km. This scheme, using fields from the coarse-resolution ECMWF data as input, appears to have some potential for determining the horizontal detail of rainfall variations caused by flow over New Zealand's rugged topography.

In view of the subjective agreement between precipitation diagnoses and satellite imagery, and the fact that ascent was diagnosed where rainfall actually fell, we proceeded to examine resolvable physical processes that contributed to ascent over northern New Zealand. A QG diagnosis suggested that ascent occurred where appreciable upper-level vorticity advection and increasing low-level thermal advection acted in phase, despite the tendency for these terms to cancel. Ascent was augmented by in situ diabatic heating.

Comparison with 200-hPa charts (Fig. 6) revealed that ascent chiefly occurred in the region between the difluent exit region of a westerly jet to the north of Bola and the confluent entrance to the second jet southeast of the SI. A cross section (Fig. 13) through this double upper-jet configuration revealed two jet-related vertical circulation features having an ascent branch in common, suggesting interaction of the transverse circulations associated with these two jets. These were a thermally direct circulation about the confluent jet entrance over the SI and an indirect one about the westerly jet exit. This double jet pattern and associated two-cell vertical circulation pattern is similar to that described by Uccellini and Kocin (1987) in association with heavy snow events over the eastern United States.

Finally, low-level processes conducive to ascent and precipitation were observed to the east of the NI. In the confluence where warm, moist northeasterly flow met a cooler southeasterly flow from about the ridge over the SI, frontogenesis and moisture convergence were diagnosed at 850 hPa. It is likely that orographic channeling locally enhanced these processes near the Gisborne Ranges, although this could not be confirmed because of the lack of observations.

One major conclusion from this study is that orographic influences dominated the observed rainfall patterns. Current knowledge about the effect of New Zealand's mountains on rainfall is largely qualitative or statistical. The operational numerical weather prediction models in use there currently lack the resolution to realistically represent the effect of the mountains on precipitation. A mesoscale model, currently under development at the National Institute of Water and Atmospheric Research, should result in improved forecasts of these crucial rainfall variations. Research is needed to determine the dynamics of flow over topography in a variety of conditions, and the role of cloud microphysics. Case studies should examine the detailed interactions that occur when large-scale weather systems impinge on this topography. The southern alps of the SI, an extreme case of a substantial mountain barrier intruding into the atmosphere from marine surroundings, are a unique natural laboratory to study these effects. Further research in that area involving detailed raingage and radar measurements and mesoscale modeling is currently being planned.

Acknowledgments. The author is grateful to Cliff Revell for critical comments on an earlier draft of this paper, and to the referees for their useful comments that helped to focus this work. The Bola rainfall dataset was kindly made available by Craig Thompson. This research was supported by the New Zealand Foundation for Research, Science and Technology Contract MET105.

REFERENCES

Anderssen, E., 1989: Impact of sounding data in the ECMWF system. *Use of Satellite Data in Operational Numerical Weather Prediction: 1989–1993, ECMWF/EUMETSAT Workshop,* ECMWF.

Bosart, L. F., and F. H. Carr, 1978: A case study of excessive rainfall centered around Wellsville, New York, 20–21 June 1972. *Mon. Wea. Rev.,* **106,** 363–374.

——, and D. B. Dean, 1991: The Agnes rainstorm of June 1972: Surface feature evolution culminating in inland storm redevelopment. *Wea. Forecasting,* **6,** 515–537.

Bradbury, D. L., 1957: Moisture analysis and water budget in three different types of storms. *J. Meteor.*, **14,** 559–565.

Carr, F. H., and L. F. Bosart, 1978: A diagnostic evaluation of rainfall predictability for Tropical Storm Agnes, June 1972. *Mon. Wea. Rev.*, **106,** 363–374.

Danard, M. B., 1964: On the influence of released latent heat on cyclone development. *J. Appl. Meteor.*, **3,** 27–37.

DeAngelis, R. M., and W. T. Hodge, 1972: Preliminary climatic data report—Hurricane Agnes, June 14–23, 1972. NOAA Tech. Memo., EDS NCC-1, 66 pp.

DiMego, G. J., and L. F. Bosart, 1982a: The transformation of Tropical Storm Agnes into an extratropical cyclone. Part I: The observed fields and vertical motion computations. *Mon. Wea. Rev.*, **110,** 385–411.

——, and ——, 1982b: The transformation of Tropical Storm Agnes into an extratropical cyclone. Part II: Moisture, vorticity and kinetic energy budgets. *Mon. Wea. Rev.*, **110,** 412–433.

Haltiner, G. J., and R. T. Williams, 1980: *Numerical Prediction and Dynamic Meteorology.* John Wiley and Sons, 477 pp.

Hill, H. W., 1970: The precipitation in New Zealand associated with the cyclone of early April 1968. *N. Z. J. Sci.*, **13,** 641–662.

Hoskins, B. J., I. Draghici and H. C. Davies, 1978: A new look at the ω-equation. *Quart. J. Roy. Meteor. Soc.*, **104,** 31–38.

Littlejohn, R. N., 1984: Extreme winds and forest devastation resulting from cyclone "Bernie." *Weather and Climate,* **4,** 47–52.

Palmén, E., 1958: Vertical circulation and release of kinetic energy during the development of Hurricane Hazel into an extratropical storm. *Tellus,* **10,** 1–21.

——, and E. O. Holopainen, 1962: Divergence, vertical velocity and conversion between potential and kinetic energy in an extratropical disturbance. *Geophysica,* **8,** 261–279.

Petterssen, S., 1956: *Weather Analysis and Forecasting.* Vol. 1. McGraw Hill, 428 pp.

Queney, P., 1948: The problem of airflow over mountains. A summary of theoretical studies. *Bull. Amer. Meteor. Soc.,* **29,** 16–26.

Revell, C. G., 1981: Tropical cyclones in the southwest Pacific. Misc. Pub. 170, New Zealand Meteorological Service, Wellington, New Zealand, 53 pp.

Sawyer, J. S., 1956: The physical and dynamical problems of orographic rain. *Weather,* **11,** 375–381.

Sinclair, M. R., 1993: Synoptic-scale diagnosis of the extratropical transition of a southwest Pacific tropical cyclone. *Mon. Wea. Rev.*, **121,** 941–960.

Smagorinsky, J., and G. O. Collins, 1955: On the numerical prediction of precipitation. *Mon. Wea. Rev.*, **83,** 53–68.

Smith, R. B., 1979: The influence of mountains on the atmosphere. *Advances in Geophysics,* No. 21, Academic Press, 87–230.

Tarbell, T. C., T. T. Warner, and R. A. Anthes, 1981: An example of the initialization of the divergent wind component in a mesoscale numerical weather prediction model. *Mon. Wea. Rev.*, **109,** 77–95.

Tomlinson, 1975: Cyclone Alison. Technical Information Circular No. 148, New Zealand Meteorological Service, 20 pp.

Trenberth, K. E., 1977: A diagnostic investigation of the behaviour of tropical cyclone Norman. New Zealand Meteorological Service Technical Note 231, 26 pp.

——, and J. G. Olson, 1988: An evaluation and intercomparison of global analyses from the National Meteorological Center and the European Centre for Medium-Range Weather Forecasts. *Bull. Amer. Meteor. Soc.,* **69,** 1047–1057.

Uccellini, L. W., and P. J. Kocin, 1987: The interaction of jet streak circulations during heavy snow events along the east coast of the United States. *Wea. Forecasting,* **2,** 289–308.

Wergen, W., 1987: Diabatic nonlinear normal mode initialisation for a spectral model with a hybrid vertical coordinate. Tech. Rep., No. **59,** ECMWF, 83 pp.